Preparation of hierarchical mesocrystalline DL-lysine·HCl-poly(acrylic acid) hybrid thin films

Yuan Jiang, Haofei Gong, Dirk Volkmer, Laurie Gower, Helmut Cölfen

Angaben zur Veröffentlichung / Publication details:

Jiang, Yuan, Haofei Gong, Dirk Volkmer, Laurie Gower, and Helmut Cölfen. 2011. "Preparation of hierarchical mesocrystalline DL-lysine·HCl-poly(acrylic acid) hybrid thin films." *Advanced Materials* 23 (31): 3548–52. https://doi.org/10.1002/adma.201101468.

Preparation of Hierarchical Mesocrystalline DL-Lysine·HCl–Poly(acrylic acid) Hybrid Thin Films

*Yuan Jiang, Haofei Gong, Dirk Volkmer, Laurie Gower, and Helmut Cölfen**

Structural hierarchy is a construction principle that forms the base of superior physical properties of biominerals such as bone,[1] sponges[2] and nacre.[3] Analytical methods have been applied on various length scales to clarify the structural details in biomineral samples in order to understand the inner relationships between their hierarchical structure and physical properties. An important discovery is that a large number of biominerals use nanoparticles instead of ions as building blocks.[1,4] This principle has clear advantages for living organisms since osmotic pressure caused by high ionic strength is prevented, and it is not necessary to transport large solution volumes for the sequestration of the necessary amount of ions. Nanoparticles can assemble into aligned superstructures with multiple hierarchy levels. For example, biominerals such as spines in sea urchins show single-crystalline diffraction patterns but are composed of nanoparticles.[5] Therefore, some biominerals are suggested to be obtained via non-classical crystallization routes.[5,6] The "mesocrystal" concept has been proposed to describe the structure of such crystallographically ordered superstructures employing nanoparticles as building blocks.[6b,7] Polymer controlled crystallization is the most effective route for the biomimetic synthesis of mesocrystals. Normally, isolated mesocrystals on the microscale are precipitated from the supersaturated mother liquor. Until now, it is still a challenge to grow hierarchical mesocrystals directly via a bottom-up route since such programmed hierarchical self-assembly requires face selective polymer adsorption.[8] However, even if the structural hierarchy of self-assembled nanoparticles reaches dimensions within the multi-micrometer range, the introduction of further hierarchy levels up to the macroscale (i.e., centimeters) is hardly achievable via a bottom-up approach since microscopic mesocrystals tend to sediment in the reaction vessel, thus becoming excluded from further self-assembly steps. Therefore, reaching higher levels of structural hierarchy requires further organization of nanoparticles via self-assembly routes that employ long-ranging interactions or interparticle forces. A few successful examples for the preparation of hierarchical mesocrystals are based on the evaporation of mother liquor, which utilizes capillary forces for nanoparticle alignment.[9]

Capillary forces, although not an obvious driving force in biomineralization processes, are effective to form patterned and even hierarchical structures–especially thin films–across the nano-, micro-, and macroscale. In addition, to confine the structural growth of nanoparticle superstructures on the surface, nanoparticle–substrate interactions must be slightly stronger than nanoparticle–nanoparticle interactions and stronger than nanoparticle–solvent and substrate–solvent interactions; otherwise, bulk aggregation occurs. Interestingly, the evaporation of a nanocrystal dispersion on a substrate can produce various patterned structures.[10] Both, solvent evaporation rate and interactions among nanocrystals, solvent, and substrate play crucial roles in determining the morphology of the as-prepared patterns.[11] Not only nanocrystals, but supramolecular structures could also be used as building blocks for the construction of patterned thin films.[12] A remarkable example is the synthesis of several hierarchical porphyrin patterns, which could be prepared in a controlled way via an evaporation process of the mother liquor without any additive.[12a]

Currently, it is still difficult to rationally synthesize patterned or even hierarchical thin films directly from the solution phase. One possibility for the synthesis of patterned thin films is to introduce chemical compounds (i.e., an evaporating mother liquor) onto a preexisting template, which in turn is fabricated by a lithographic or patterning route,[13] but this approach does still not introduce hierarchical ordering within the depositing materials themselves. Hierarchical mesocrystalline thin films with five hierarchical levels on a free standing substrate have been difficult to prepare so far, because the ordering of the nanoparticles into a crystallographic register is a further hurdle to be overcome in the bottom-up synthesis of hierarchical structures.[14] Herein, we describe a convenient route for the formation of mesocrystalline thin films with at least five hierarchy levels including pattern assembly, fan-shaped pattern, dendrite, fiber with branches, lamella, and nanoparticle.

The hierarchical thin film was obtained from the reprecipitation of DL-Lys·HCl microspheres (Figure S1, Supporting Information). First, DL-Lysine·HCl (DL-Lys·HCl) microspheres were prepared in a DL-Lys·HCl–poly(acrylic acid) (PAA)–water–ethanol (EtOH) system via the polymer-induced liquid precursor (PILP) route. The concept of "PILP" was put forward to explain the formation of $CaCO_3$ crystals with a $\mu g \cdot mL^{-1}$ quantity of polyacids such as polyaspartic acid and polyacrylic acid.[15] The

Dr. Y. Jiang,[+] Prof. H. Cölfen
Max Planck Institute of Colloids and Interfaces
Colloid Chemistry
Am Mühlenberg, D-14476 Golm, Germany
E-mail: helmut.coelfen@uni-konstanz.de
Dr. H. Gong, Prof. D. Volkmer
Institute of Physics
Chair of Solid State & Materials Chemistry
Augsburg University
D-86159 Augsburg, Germany
Prof. L. Gower
Materials Science & Engineering
University of Florida
Gainesville, 32611, USA
[+] Present Address: Physical Chemistry, University of Konstanz, Universitätsstr. 10, D-78457 Konstanz, Germany

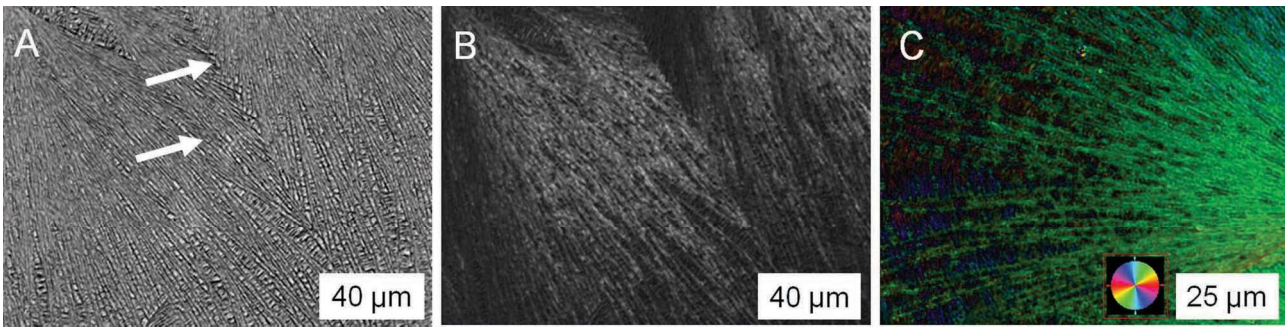

Figure 1. Panels A and B show OM and POM images, respectively. They were taken at the same area. The arrows in the image of panel A show the boundaries between patterns. Panel C shows a quantitative birefringence optical micrograph (Abrio). A difference in color in the image of panel C means various structural orientations.

crystallization passes through liquid precursors due to the existence of polymeric additives and crystals with complex shapes are obtained thereafter. The experiment herein was performed by mixing DL-Lys·HCl–PAA aqueous solution with EtOH. Due to the insolubility of DL-Lys·HCl in EtOH, the supersaturation for DL-Lys·HCl was high and the crystallization occurs. With the PAA additive, DL-Lys·HCl precipitated via the PILP route and microspheres with radially oriented nanoplatelets as building blocks were obtained. Similar microsphere structures such as charged amino acids and pigments have been successfully synthesized by using small organic molecules via a modified "drowning-out" route with the existence of oppositely charged polyelectrolytes.[16] When the as-prepared microsphere dispersion was dropped on the substrate, the solvent began to evaporate. Due to the higher vapor pressure of EtOH as compared to water, EtOH evaporated faster than water. Therefore, the EtOH/water ratio was decreasing, making the solvent increasingly better for DL-Lys·HCl. At a certain EtOH/water ratio value and solvent concentration, DL-Lys·HCl became undersaturated in the mixture and started to dissolve (see Figure S2, Supporting Information). Thereafter, a liquid thin layer was formed. The continuous solvent evaporation caused the supersaturation of DL-Lys·HCl in the mixture, which resulted in the reprecipitation of DL-Lys·HCl into hierarchical thin films in presence of PAA.[11] Without any external template, the as-prepared hierarchical thin films show high orientation in parallel to the substrate.

Different microscopic techniques provide structural details of the as-prepared hierarchical thin films on the macro- and microscale. **Figure 1**A is an optical microscopy (OM) image, showing an overview of a patterned thin film (level one) on the hydrophilic glass slide. The thin film is a patterned assembly and is composed of many fan-shaped patterns (level two), which are hundreds of micrometers in size. The structural density within each fan-shaped pattern is heterogeneous. The structures grow in a radial direction and the structural density is getting lower along the growth direction of each fan-shaped pattern (Figures S3A-B, Supporting Information). Fan-shaped patterns stop growing when they meet the neighboring one. The boundary between fan-shaped patterns is visible in Figure 1A. The same area observed by polarized OM (POM) shows a bright color, indicating that the thin film contains highly ordered structures. The x-ray diffraction (XRD) pattern later on shows that the thin film is crystalline.

Sub-structures can be observed within each fan-shaped pattern, as shown in Figure 1A and Figure S3 (Supporting Information). They are dendritic structures (level three). Within each growing fan-shaped pattern, several dendrites grow perpendicular to the main axis towards the center of the fan-shaped pattern. The branches are growing in length along the growth direction of the dendrites. The width of each branch can be as long as 60 µm near to the end of each growing dendrite (Figure S3B, Supporting Information). Therefore, the heterogeneity of fan-shaped patterns is due to the growing width of branches in each dendrite along the growth direction of dendrites. Dendritic structures are usually obtained via a far from equilibrium self-organization process, and they exist in minerals, snowflakes and nanocrystal superstructures.[17]

To understand the orientation effect in the thin film, quantitative birefringence imaging microscopy technique (Abrio) was used to detect the inner orientation within each fan-shaped pattern. The imaging system measures the retardance magnitude at every pixel of a charge-coupled device image. Therefore, it can provide quantitative information about the orientation of each polycrystalline grain. The orientation difference can be shown in different colors as shown in an example in Figure 1C. Therein, the color on the right side is green, and the color is switching to partly blue along the clockwise direction. This result suggests that fan-shaped patterns are spherulitic in nature and each main axis in the dendrite is nearly iso-oriented. The area filled with branches on the left side shows a red-purple color. Therefore, the orientation of branches is vertical to the axis. More details will be discussed later in combination with the atomic force microscopy (AFM) and XRD results.

AFM was applied to provide more structural details of the hierarchical thin films on the micro- and nano-scale. **Figure 2**A shows the coexistence of several dendrites on the microscale. Fibers can be separated into two along the growth direction of dendrites (see arrows in Figure 2A). Branches align themselves vertical to the fibers. Figure 2B provides the structural details of fibers and branches. It indicates that both fibers and branches are lamellar assemblies (level four). The main fibers contain two lamellae (level five) in parallel. Each branch contains several lamellae adhered in parallel along the axis direction. The width of the lamellae is ~40–80 nm, as shown in Figure 2C. The same image proves that each lamella is a nanostructure assembly. The size of the nanostructure on top ~40–80 nm is equal to the width of the lamellae.

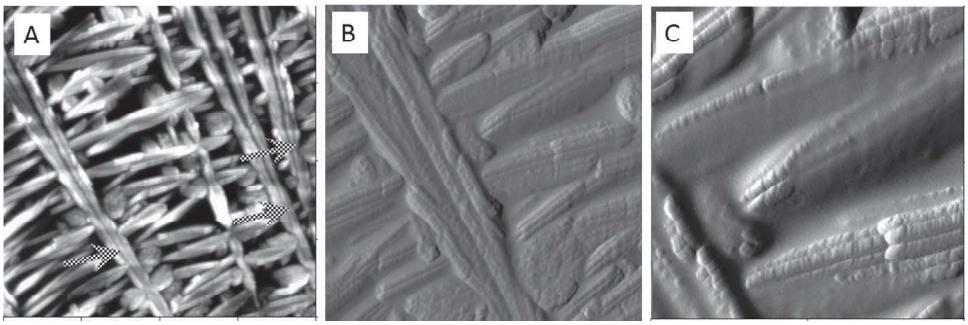

Figure 2. Three AFM images indicate the hierarchy levels from the micro- to the nano-scale. The scales of the images in panels A, B, and C are 10, 4, and 2 µm, respectively. Panel A shows a height image, while panels B and C show amplitude images for clarification reasons. In panel C, the nanoparticles making up the fibers (level 4) can be observed. Three arrows in panel A show the areas, where each fiber splits into two.

The thin film was crushed by using sharp tweezers tips at room tempearture (RT) to clarify structural details underneath the thin film surface. Spherical nanoparticles were clearly observable on the surface (Figure S4, Supporting Information). Therefore, the building blocks of the hierarchical thin films are nanoparticles (level six) and they assemble into lamellae in fibers with branches.

XRD was applied to understand the crystalline structures in the hierarchical thin film and their orientation. Judging from the XRD diffractogram in **Figure 3**A, the hierarchical thin film is polycrystalline. Thin film and DL-Lys·HCl microspheres precipitated directly from a water-EtOH mixture show the same polymorph (an orthorhombic space group $Pc2_1/c$ with a unit cell parameters: a = 9.157 Å, b = 11.166 Å, c = 8.547 Å, β = 105.83°; index N.O.: 00-047-1985 I). However, it is obvious that the hierarchical thin film is also highly oriented. Only four peaks from the {a 0 0} family (where a = 1, 2, 3, and 4) are visible in the XRD pattern detected for the hierarchical film. Therefore, XRD data suggest that both fibers and branches grow preferentially along the [100] axis in the hierarchical thin film. The almost perfect orientation of the nanocrystals is surprising since the glass surface used for film formation is not structured at all. Indeed, the microspheres used for the preparation of the hierarchical thin films do not show any orientation effect (Figure 3a red curve). The reason for the observed [100] orientation in the thin films obtained via a PILP precursor might be nanoparticle alignment by dipole fields, which will be discussed below.

The molecular structure of a DL-Lys·HCl crystal can help to understand the interactions between DL-Lys·HCl and PAA. By depicting a (100) surface cut of DL-Lys·HCl, (Figure 3B) we found that the (100) surface can be purely positively but also purely negatively charged either exposing carboxyl groups or chlorine ions. Therefore, the carboxyl groups on deprotonated PAA molecules cannot interact with a negatively charged (100) DL-Lys·HCl surface via electrostatic interactions. On the other hand, (010) and (001) surfaces can also be positively charged due to the exposed amine groups (Figures S5A-B, Supporting Information), and for these surfaces, a cut with a purely negative surface is not possible. Therefore, both (010) and (001) are positively charged surfaces which can interact with PAA and will thus not get exposed. This can explain the observed preferential [100] orientation. Another specialty of the [100] axis is that it can be dipolar due to the orientation of the DL-Lys·HCl

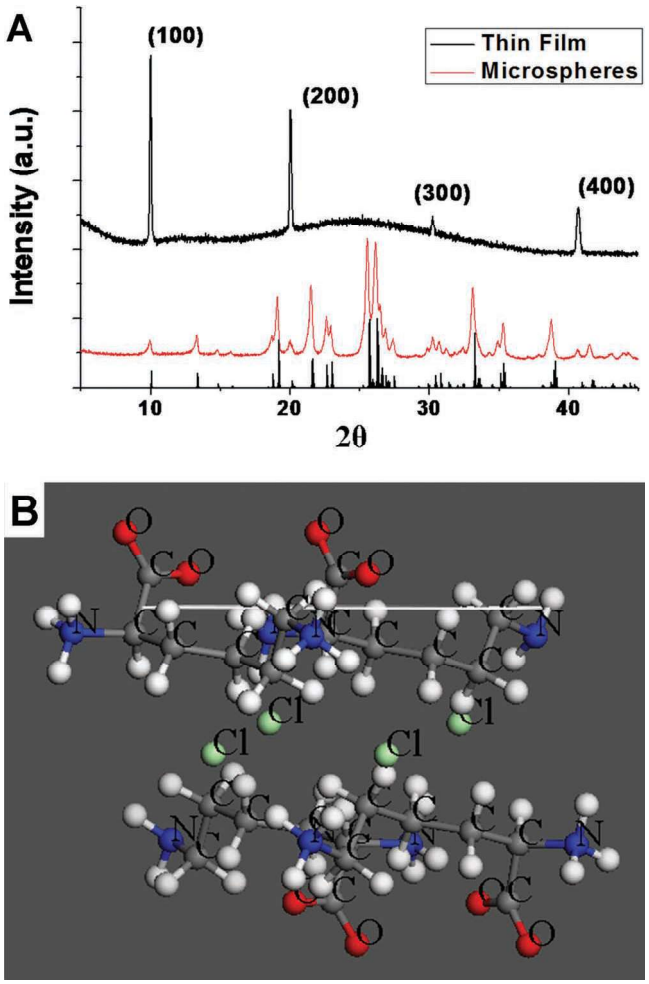

Figure 3. Panel A shows three XRD patterns from a hierarchical thin film (top, black), microspheres (middle, grey; see microspheres in Figure S1, Supporting Information) and the standard XRD data of DL-Lys·HCl (bottom, black columns). In panel B, the line represents the (100) surface of DL-Lys·HCl. The groups exposed from the (100) surface are carboxyl groups. Those isolated spots between two molecular layers are Cl^-. H atoms are not labeled for clarity reasons (Blue = N, red = O, gray = C, and green = Cl^-; an orthorhombic space group $Pc2_1/c$ with unit cell parameters: a = 9.157 Å, b = 11.166 Å, c = 8.547 Å, β = 105.83°; index N.O.: 00-047-1985 I.

molecules if a defect leads to the exposition of carboxyl and amine groups on opposite sites. Both fibers and branches are mesocrystalline as evidenced by combination of Abrio, AFM, SEM and XRD results. First, SEM and AFM proved that the building blocks of the hierarchical thin film were nanoparticles. These nanoparticles are crystalline and according to XRD patterns show crystallographic orientation as further evidenced by polarization microscopy. Therefore, fibers and branches are mesocrystals and show the same orientation preference of [100] according to the XRD results.

We combined a novel reprecipitation route with an evaporation process for the construction of hierarchical mesocrystalline thin films. The chemical structure of the deposited sample (colloids or molecules), in combination with the evaporation process, is responsible for the determination of the pattern morphology.[11] Herein, the existence of the second solvent–EtOH and the polyanionic additive–PAA fine tuned the precipitation process, resulting in the formation of patterns with at least five hierarchy levels. EtOH played several key roles during the formation of the hierarchical thin films. As a non-solvent for DL-Lys·HCl and PAA, EtOH led to the homogeneous nucleation of nanoplatelets, which self-organized into microspheres (Figure S1, Supporting Information). EtOH also confined the growth to the substrate instead of a growth of 3D structures by wetting the substrate surface. Indeed, K_2SO_4/PAA hierarchical crystals were obtained by evaporating K_2SO_4–PAA aqueous solution in a beaker, where there was not enough driving force for 2D growth along the substrate.[9b] Therefore, a slow water evaporation rate was responsible for an oscillating growth mode between 2D and 3D on different size scales. We also observed that direct evaporating DL-Lys·HCl/PAA aqueous solution on the glass slide caused the fabrication of isolated ring stains, which showed the oscillation of 2D and 3D growth mode (Figure S6, Supporting Information). As a third role, EtOH has a larger vapor pressure compared to water. The faster evaporation rate of EtOH increased the solvent quality for the solutes and led to a dissolution- reprecipitation mechanism.

PAA is also an independent ingredient for the formation of hierarchical thin films for two reasons. Performing a reference experiment without PAA, we obtained randomly oriented and isolated classical single crystals nucleated directly on the hydrophilic glass slides (Figure S7, Supporting Information). PAA, as a polyanion countercharged to the positively charge DL-Lys·HCl, is primarily responsible for stabilizing nanocrystals from an Ostwald ripening process. This is realized by adsorbing PAA onto the growing (010) and (001) surfaces of DL-Lys·HCl but also partly onto (100) in case a positive surface charge is exposed. The dipoles of DL-Lys·HCl along the [100] direction can sum up to a large value by reorienting the nanocrystals along the same direction. Therefore, mesocrystalline thin films were obtained aligned along the [100] axis. AFM results showed that there was no separated PAA phase, suggesting that all PAA was involved in the formation of the nanocrystals. By dissolving the thin film with D_2O, we determined that the value of DL-Lys·HCl/PAA (w/w) at ~10 by using NMR spectroscopy, which was equal to the initial value (data are not shown).

Mesocrystalline thin films with at least five hierarchy levels were prepared successfully. DL-Lys·HCl precipitated into nanoparticles with the protection from the polyanionic additive PAA during the evaporation of the EtOH/water solvent mixture. Nanoparticles self-assembled into lamellae composed of mesocrystals micrometers in size. Due to the fast evaporation rate of the solvent, mesocrystals self-assembled into 2D dendrites, which could further form fan-shaped thin films. The evaporation process nicely formed the hierarchical thin films on the macroscale with mesocrystals as building blocks. The results herein prove that it is possible to combine the mesocrystal and PILP concepts with other physical forces for the formation of complex even hierarchical thin films by precisely controlling the processing parameters. In addition, the similar procedure can be extended to L-Lys·HCl/PAA systems (Figure S8, Supporting Information). The hierarchical thin films presented herein show several similarities to biological structures such as fern structures. Investigation of the formation mechanism of the hierarchical thin films is the key for the rational design of further artificial thin films with complex structures.

Experimental Section

Chemicals and Materials: DL-Lys·HCl (DL-Lys·HCl) 98% in purity was purchased from Aldrich. Poly(acrylic acid) (PAA; average M_W = ~2000 g·mol^{-1}; 63 wt% aqueous solution contains 47 wt% acrylic resin, 16 wt% sodium polyacrylate, and 37 wt% water; pH = 2.2–3.0) was purchased from Acros Organics. Both chemicals were used directly without any further purification. EtOH Absolute (HPLC grade) was purchased from Merck. Double distilled water was used for the preparation of aqueous solutions. Microscope cover glasses 10 mm in diameter were purchased from Fisher Scientific. The glass slides were rinsed in a solution by mixing equal volume of concentrated H_2SO_4 (96–98 wt%) and aqueous H_2O_2 solution (40 wt%) at RT for 24 hours. Double distilled water was used for the storage of clean glass slides.

Preparation of Microspheres: First, an aqueous solution containing 70 mg·mL^{-1} DL-Lys·HCl and 7 mg·mL^{-1} PAA was prepared at RT. After the complete dissolution of DL-Lys·HCl and PAA, the aqueous solution was quickly mixed with EtOH 1/9 (v/v) at room temperature. The mixture was gently shaken for seconds for complete mixing. The reaction proceeded for 24 hours for the complete precipitation of DL-Lys·HCl microspheres. The microspheres sedimented to the bottom and the supernatant was clear.

Preparation of Thin Films: The as-prepared DL-Lys·HCl microsphere dispersion was sonicated for 1 min. The mixture turned turbid because microspheres were nearly homogeneously distributed in the mixture. Then, 21 µL of above mixture was quickly transferred by a micropipette onto the microscope cover glass. The cover glass was left at RT for the evaporation of solvent, the dissolution of microspheres and the growth of hierarchical thin films. The experiments were performed when the humidity was between 20% and 30%. It took three days before the sample was used for characterization.

Characterization: The as-prepared sample on the glass slide was placed under a Leica DMRB microscope with polarizers for the scanning. Light micrographs were taken with a Leica DMRB microscope and a birefringence microscope (Abrio). The SEM measurements were performed on a LEO 1550 GEMINI. AFM images were recorded on a multimode AFM machine with tapping mode from Veeco Instruments. X-ray diffraction data were recorded on a Bruker D8 advance diffractometer.

Supporting Information

Supporting Information is available from the Wiley Online Library or from the author.

Acknowledgements

This work was supported by the DFG & NSF "Materials World Network to Study Liquid Precursor Formation and Crystallization at Interfaces:

Fundamentals towards Applications." Y.J. thanks The Max Planck Institute of Colloids and Interfaces for the financial support during 2008-2010. Y.J. acknowledges Rona Pitschke, Heike Runge, and Dr. Jürgen Hartmann for SEM measurements, Anneliese Heilig for AFM measurements, and Dr. Nicola Pinna for providing the necessary crystal data.

[1] S. Weiner, H. D. Wagner, *Annu. Rev. Mater. Sci.* **1998**, *28*, 271–298.
[2] J. Aizenberg, J. C. Weaver, M. S. Thanawala, V. C. Sundar, D. E. Morse, P. Fratzl, *Science* **2005**, *309*, 275–278.
[3] B. L. Smith, T. E. Schaffer, M. Viani, J. B. Thompson, N. A. Frederick, J. Kindt, A. Belcher, G. D. Stucky, D. E. Morse, P. K. Hansma, *Nature* **1999**, *399*, 761–763.
[4] M. Rousseau, E. Lopez, P. Stempfle, M. Brendle, L. Franke, A. Guette, R. Naslain, X. Bourrat, *Biomaterials* **2005**, *26*, 6254–6262.
[5] Y. Oaki, A. Kotachi, T. Miura, H. Imai, *Adv. Funct. Mater.* **2006**, *16*, 1633–1639.
[6] a) F. C. Meldrum, H. Cölfen, *Chem. Rev.* **2008**, *108*, 4332–4432; b) H. Cölfen, M. Antonietti, *Mesocrystals and Nonclassical Crystallization*, John Wiley & Sons Ltd, Chichester **2008**.
[7] a) H. Cölfen, S. Mann, *Angew. Chem. Int. Ed.* **2003**, *42*, 2350–2365; b) H. Cölfen, M. Antonietti, *Angew. Chem. Int. Ed.* **2005**, *44*, 5576–5591.
[8] S.-H. Yu, H. Cölfen, K. Tauer, M. Antonietti, *Nat. Mater.* **2005**, *4*, 51–55.
[9] a) Y. Oaki, H. Imai, *Chem. Commun.* **2005**, 6011–6013; b) Y. Oaki, H. Imai, *Adv. Funct. Mater.* **2005**, *15*, 1407–1414.
[10] a) E. Adachi, A. S. Dimitrov, K. Nagayama, *Langmuir* **1995**, *11*, 1057–1060; b) P. C. Ohara, J. R. Heath, W. M. Gelbart, *Angew. Chem. Int. Ed.* **1997**, *36*, 1078–1080; c) A. Sharma, R. Khanna, *Phys. Rev. Lett.* **1998**, *81*, 3463–3466; d) P. Moriarty, M. D. R. Taylor, M. Brust, *Phys. Rev. Lett.* **2002**, *89*, 4; e) E. Rabani, D. R. Reichman, P. L. Geissler, L. E. Brus, *Nature* **2003**, *426*, 271–274; f) J. X. Huang, F. Kim, A. R. Tao, S. Connor, P. D. Yang, *Nat. Mater.* **2005**, *4*, 896–900; g) T. P. Bigioni, X. M. Lin, T. T. Nguyen, E. I. Corwin, T. A. Witten, H. M. Jaeger, *Nat. Mater.* **2006**, *5*, 265–270; h) C. P. Martin, M. O. Blunt, E. Pauliac-Vaujour, A. Stannard, P. Moriarty, I. Vancea, U. Thiele, *Phys. Rev. Lett.* **2007**, *99*, 4.
[11] a) R. D. Deegan, O. Bakajin, T. F. Dupont, G. Huber, S. R. Nagel, T. A. Witten, *Nature* **1997**, *389*, 827–829; b) V. Palermo, P. Samori, *Angew. Chem. Int. Ed.* **2007**, *46*, 4428–4432.
[12] a) R. van Hameren, P. Schon, A. M. van Buul, J. Hoogboom, S. V. Lazarenko, J. W. Gerritsen, H. Engelkamp, P. C. M. Christianen, H. A. Heus, J. C. Maan, T. Rasing, S. Speller, A. E. Rowan, J. Elemans, R. J. M. Nolte, *Science* **2006**, *314*, 1433–1436; b) X. H. Fang, B. Q. Li, E. Petersen, Y. S. Seo, V. A. Samuilov, Y. Chen, J. C. Sokolov, C. Y. Shew, M. H. Rafailovich, *Langmuir* **2006**, *22*, 6308–6312; c) C. Y. Zhang, X. J. Zhang, X. H. Zhang, X. Fan, J. S. Jie, J. C. Chang, C. S. Lee, W. J. Zhang, S. T. Lee, *Adv. Mater.* **2008**, *20*, 1716–1720.
[13] a) J. Aizenberg, A. J. Black, G. M. Whitesides, *Nature* **1999**, *398*, 495–498; b) N. Gehrke, N. Nassif, N. Pinna, M. Antonietti, H. S. Gupta, H. Cölfen, *Chem. Mater.* **2005**, *17*, 6514–6516; c) A. L. Briseno, S. C. B. Mannsfeld, M. M. Ling, S. Liu, R. J. Tseng, C. Reese, M. E. Roberts, Y. Yang, F. Wudl, Z. Bao, *Nature* **2006**, *444*, 913–917; d) Y. Y. Kim, E. P. Douglas, L. B. Gower, *Langmuir* **2007**, *23*, 4862–4870.
[14] a) C. Sanchez, B. Julian, P. Belleville, M. Popall, *J. Mater. Chem.* **2005**, *15*, 3559–3592; b) E. V. Shevchenko, D. V. Talapin, N. A. Kotov, S. O'Brien, C. B. Murray, *Nature* **2006**, *439*, 55–59.
[15] a) L. A. Gower, D. A. Tirrell, *J. Crystal Growth* **1998**, *191*, 153–160; b) L. B. Gower, D. J. Odom, *J. Crystal Growth* **2000**, *210*, 719–734; c) L. B. Gower, *Chem. Rev.* **2008**, *108*, 4551–4627.
[16] a) S. Wohlrab, H. Cölfen, M. Antonietti, *Angew. Chem. Int. Ed.* **2005**, *44*, 4087–4092; b) Y. R. Ma, G. Mehltretter, C. Plug, N. Rademacher, M. U. Schmidt, H. Cölfen, *Adv. Funct. Mater.* **2009**, *19*, 2095–2101.
[17] a) J. S. Langer, *Science* **1989**, *243*, 1150–1156; b) H. Imai, in *Biomineralization I: Crystallization and Self-Organization Process*, Vol. *270*, Springer-Verlag Berlin, Berlin, **2007**, pp. 43–72.